STM JOURNALS

Research & Reviews: Journal of
Physics

https://journals.stmjournals.com/rrjophy

ISSN: 2278-2265 (Online)
ISSN: 2347-9973 (Print)
Volume 14, Issue 1, 2025
January–April
DOI (Journal): 10.37591/RRJoPHY

Review RRJoPHY

Influence of Horizontal Crossflow on the Rayleigh-Taylor Instability: A Numerical Approach

Rakesh Roshan Apatta[1], Santosh Kumar Panda[2],
Basanta Kumar Rana[3,*], Jnana Ranjan Senapati[4]

Abstract

Rayleigh-Taylor Instability (RTI) is a typical occurrence in natural events, engineering, and industrial applications. When the lighter fluid (bottom medium) is forcing the heavier fluid (top medium) on top of the lighter fluid because of a gravitational field, then that phenomenon is called Rayleigh-Taylor instability (RTI). Despite extensive records of investigating this common phenomenon i.e., RTI with several unique boundary conditions, apparently, there are no prior investigations for the RTI with horizontal crossflow effect. In this paper, numerical simulations have been performed using volume of fluid (VOF) method for the reorientation of the interface. Here, we have chosen an open-source Gerri's software for this RTI phenomenon to execute all the investigations. In this situation, the physical boundary that permits the exchange of certain entities between two phases (lighter and heavier fluid) is known as the interface. The region where it primarily emerges is the layer of stability between phases that permits the progressive transmission of constrained entities established as the result of an emphasis on the dominant influence. This study reveals how the horizontal crossflow of the top medium, which is a heavier fluid, as well as the density ratio (ρ_r) established deviations in the complex interfacial structures. Horizontal crossflow of the upper layer (heavier fluid) has been expressed by the non-dimensional number, Reynolds number (Re_f). The variation in the vertical (Y) and angular positions (θ) of the spike from the initial undisturbed interface is also a topic of this present investigation. To examine the flow patterns closer to the interface, we displayed velocity vector diagrams for various combinations of Reynolds number (Re_f) and density ratio (ρ_r).

Keywords: Rayleigh-Taylor instability, spike, horizontal crossflow, Reynolds number, density ratio

***Author for Correspondence**
Basanta Kumar Rana
E-mail: basanta.uce@gmail.com

[1]Ph.D. Research Scholar, School of Mechanical Engineering, Kalinga Institute of Industrial Technology (KIIT) Deemed to be University, Bhubaneswar, Odisha, India.
[2]Assistant Professor, Department of Mechanical Engineering, Atria Institute of Technology Bengaluru, Karnataka, India
[3]Assistant Professor, School of Mechanical Engineering, Kalinga Institute of Industrial Technology (KIIT) Deemed to be University, Bhubaneswar, Odisha, India.
[4]Assistant Professor, Department of Mechanical Engineering, National Institute of Technology, Rourkela, India

Received Date: February 05, 2025
Accepted Date: February 10, 2025
Published Date:

Citation: Rakesh Roshan Apatta, Santosh Kumar Panda, Basanta Kumar Rana, Jnana Ranjan Senapati. Influence of Horizontal Crossflow on the Rayleigh-Taylor Instability: A Numerical Approach. Research & Reviews: Journal of Physics. 2025; 14(1): 1–11p.

INTRODUCTION

When the lighter fluid (bottom medium) is forcing the heavier fluid (top medium) on top of the lighter fluid because of a gravitational field, then that phenomenon is called to be Rayleigh-Taylor instability (RTI). It generally develops at the interface between the two fluids of different densities [1]. Generally, Rayleigh [2] examined first about the RTI in a fluid with the help of gravitational effect. After that, Taylor [3] further extended this RTI phenomena to many fluids with the help of acceleration effect. In a variety of geophysical, engineering and aerospace related applications, and astrophysical flows [1], atmospheric physics [4], chemical reactor process [5], oceanography [6], atomic bomb blast [7], supernova remnant [8], supernova star blast [9], and cosmic and stellar dynamics related applications [10], the RTI is very crucial. Thus, it is crucial to develop a precise and effective numerical methodology for the RTexplain natural occurrences and commercial applications. Numerous researchers have carried out numerous experimental and numerical studies for the RTI [1-17]. The fingers which include bubbles and spikes, of heavier fluid penetrating into the lighter fluid medium are the real evidence of RT instability. The bubble formation and development and turbulent mixing are caused because of RTI with initial random disturbances [1]. Tian and Yuan [11] adopted the Runge-Kutta discontinuous Galerkin approach for simulating the RTI problem with large density ratios. Based on the incompressible smoothed particle hydrodynamics technique, Rahmat et al. [12] computationally investigated about the external electric filed for the RTI analysis. Using diffuse interface methodology, Ding et al. [13] used higher density ratios in incompressible two-phase flows for RTI problem. Using a phase-field based lattice Boltzmann hypothesis, Zu, and He [14] investigated the variations/alterations of density and viscosity for incompressible binary fluid systems Xiang et al. [15] numerically investigated about disintegration of gas-liquid interface by employing shear-layer flows to the both the phases. To carry out all the simulations using the volume of fraction (VOF) method, they have employed the free open source Gerris software. Later, the Rayleigh-Taylor instability phenomenon is widely used to explain rotational induced occurrences [16-29]. Panda et al. [16] analyzed about the interaction between rotational flux and horizontal crossflow of gaseous medium which generally causes a significant impact on the liquid wrapping thickness and air entrainment thickness for various combinations of immiscible gas-liquid pairs. They looked into the effects of the Capillary number $(Ca = \mu_l \omega D/2\sigma)$ and Archimedes number $\left(Ar = gD^3\rho_l^2/\mu_l^2\right)$ on the configuration of the interfacial layer, and they also discovered the formation of spherical gas bubbles from air filaments. To illustrate the dynamics of cusp-shaped entrained air filaments due to the same speed and counter-rotating solid horizontal rollers with an additional effect of horizontal crossflow on the gaseous phase, Panda, and Rana [20-21] has employed two counter rotating cylinders that are completely submerged in a highly viscous liquid pool. They also established that formation of upper rounded crest type structure due to lower speed of rollers, [27] as well as reduction in horizontal distance between rollers. Panda and Rana [28] illustrated about development of cusp-shaped air filament structure inside a liquid viscous pool because of two vertically aligned clockwise revolving rollers arrangement. They noticed some noteworthy interfacial characteristics and divided them into three zones by altering the submerged depth (W/D). Namely, the no-effect (single roller), the bent filament,[29] and the cuspoidal filament zone. After a careful investigation of previous studies, we developed a computational model for Rayleigh–Taylor instability (RTI) by employing horizontal crossflow $\left(Re_f\right)$ in the heavier fluid (top medium) for analysis of interesting and complex interfacial structures.

OBJECTIVES OF PRESENT RESEARCH

The prime research of this investigation is to understand the dynamics of interfacial configurations in presences of additional horizontal cross flow of heavier fluid, and the effect of Re_f and ρ_r vertical $\left(Y(\text{m})\right)$ and angular $\left(\theta(\text{degree})\right)$ positions of interfacial configurations. Finally, we exhibited velocity vectors for different combinations of Re_f and ρ_r to anticipate the interfacial dynamics by observing the flow patterns near the interface.

NUMERICAL METHODOLOGY

Computational domain

Using a Eulerian approach-based volume of fluid (VOF) framework, numerical simulations of the Rayleigh-Taylor instability problem have been carried out with the supplementary effect of uniform steady horizontal cross flow (U) of heavier fluid (top medium). The energy equation is neglected since it is assumed that the flow (U) in this situation is isothermal/ temperature independent. A non-dimensional number i.e. Reynolds number $\left(Re_f = \rho_h UL/\mu_h\right)$, where ρ_h and μ_h are the density and viscosity of the heavier fluid, and L is the width of the computational domain, is used to delineate the uniform steady horizontal cross flow (U) passing over left to right side of top medium (heavier fluid). The simulation domain is depicted symmetrically in Figure 1(a) as being 1m × 4m, with the heavier fluid is in the top and the lighter fluid is in the bottom medium. Two phases are often separated by an initial sinusoidal interface that is translated by 0.5 along the positive y-axis, and uniform steady horizontal cross flow (U) has employed to top medium (heavier fluid) from left to right portion. In this case, we used the free open-source Gerris solver (Popinet [30]) and a multilevel, adaptive, structured mesh to carry out the current investigation as shown in Figure 1(b). For the present study, incompressible Newtonian fluid pairs are used, and the corresponding parameters are listed in Table 1.

Table 1. Fluid properties [11] adapted for the present simulation.

Rayleigh-Taylor instability	Name of the fluid	ρ (kg/m^3)	μ (Pa. s)	g (m/s^2)
	Heavier fluid	1.225	0.00313	9.81
	Lighter fluid	0.1694		

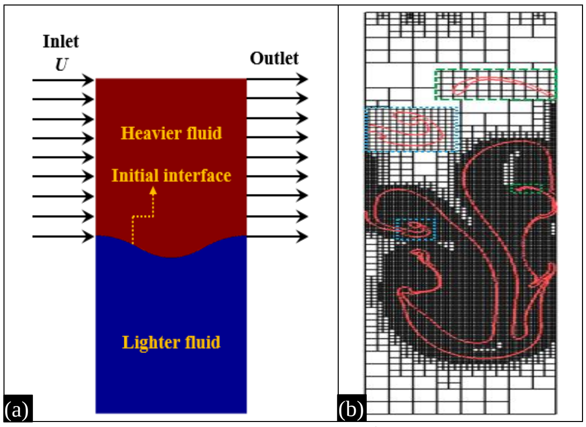

Figure 1. (a) Schematic representation of computational domain for Rayleigh-Taylor instability, and (b) assessment of adaptive cells based on the gradient of volume fraction.

Formulation of the Problem

In the current study, Gerris solver (Popinet [30]) is employed to locate and observe intriguing interfacial structures for the Rayleigh-Taylor instability problem. We commonly employed a Volume of Fluid (VOF) based technique that comprises an incompressible and density-based Navier-Stokes solver to computationally estimate complex interfacial structures. Here, momentum, continuity equations as well as body and surface forces are shown as follows:

$$\rho\left(\frac{\partial u_i}{\partial t}+u_j\frac{\partial u_i}{\partial x_j}\right)=-\frac{\partial p}{\partial x_j}+\frac{\partial}{\partial x_j}\left[\mu\left(\frac{\partial u_i}{\partial x_j}+\frac{\partial u_i}{\partial x_i}\right)\right]+\sigma k\delta_s n \quad (1)$$

$$\frac{\partial p}{\partial t}+\nabla.(\rho u)=0 \quad (2)$$

Equation (2) can be transformed into the appropriate form at outside of the interfacial regime by considering fluid density remains constant:

$$\frac{\partial u_i}{\partial x_i}=0 \quad (3)$$

Therefore, the density of fluid, velocity, and dynamic viscosity are $\rho=\rho(x,t)$, $u_i=(u,v)$, and $\mu=\mu(x,t)$ respectively. The interfacial dynamics are involved with by the Dirac distribution function δ_s (a surface tension term), where k, n, and σ are the curvature, normal to the heavier-lighter fluid interface, and coefficient of surface tension, respectively.

Using the volume fraction term $c(x,t)$, the density and viscosity of a generalised fluid at locations are as follows:

$$\rho(\hat{\alpha}) = \hat{\alpha}\rho_h + (1 - \hat{\alpha})\rho_l \quad (4)$$

$$\mu(\hat{\alpha}) = \hat{\alpha}\mu_h + (1 - \hat{\alpha})\mu_l \quad (5)$$

The abbreviations ρ_l, μ_l, ρ_h and μ_h, respectively, stand for the densities and viscosities of lighter and heavier fluid phases.

Equation (2) can be changed to give the volume fraction term shown below:

$$\frac{\partial \alpha}{\partial t} + \nabla.(\alpha u) = 0 \quad (6)$$

The above equations 1, 2, and 6 are discretized through a second-order accurate staggered spatial grid technique.

Validation

We have compared the present vertical positions $\left(Y(\mathrm{m})\right)$ of the spike from initial undisturbed interface to earlier literatures for achieving the goal of performing the validation process, particularly Ding et al. [13] and Zu and He [14]. For an appropriate comparison, the simulations have been performed using the identical fluid pair, density ratio (ρ_r), and domain range ($1\mathrm{m} \times 4\mathrm{m}$) for the Rayleigh–Taylor instability problem. Figure 2 reveals that the outcomes of our simulation are closely linked to the earlier studies, which validates our present research and provides confirmation for subsequent investigations.

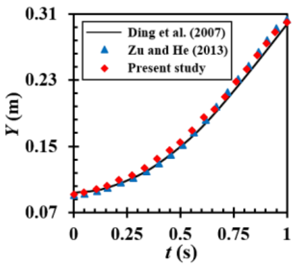

Figure 2. A comparison of the current vertical spike positions $\left(Y(\mathrm{m})\right)$ from initial undisturbed interface with those reported in earlier studies (Ding et al. [13], and Zu and He [14]).

RESULTS AND DISCUSSION

The present section describes the dynamics and behaviour of Rayleigh-Taylor instability in presences of horizontal cross flow on heavier fluid phase (presented in terms of Re_f) for various time stamps ($t = 0 - 1$ s). The present section not only describes the influence of horizontal cross flow of heavier fluid (top medium) on interfacial configurations but also depicts the effect of density ratio (presented in terms of ρ_r) on Rayleigh-Taylor instability. Some fundamental plots have been exhibited from base simulations to show the effect of the horizontal cross flow and density ratio on vertical $\left(Y(\mathrm{m})\right)$ and angular position $\left(\theta(\mathrm{degree})\right)$ of interfacial configurations. Finally, we have shown the velocity vectors diagram to visualise the flow patterns for Rayleigh-Taylor instability.

The section initiation with the variation of steady numerical contours of Rayleigh-Taylor instability for various horizontal cross flow $\left(Re_f\right)$ of heavier fluid, which is allocated in the top medium. Presently, we have displayed temporal evolutions of interfacial configurations considering various horizontal cross flows (Figure 3). The behaviour and structure of the Rayleigh-Taylor instability is elucidated comprehensively with/without the supplementary effect of the horizontal crossflow of a heavier fluid. The chosen density ratio ($\rho_r = \rho_1/\rho_2$, where ρ_1 and ρ_2 are the density of ligher and heavier fluid respectvely) has been considered to be constant ($\rho_r = 7.23$) for this instant (Figure 3). It has been clearly noticed that the interfacial length of Rayleigh-Taylor instability is progessively rise with progress of time for a particular Re_f (Figure 3 (f-j)) and also the interfacial configuration shifts more towards right side with progress of time (Figure 3 (i-j, n-o, and s-t) comparing with no horizontal cross flow case (Figure 3 (d-e)). This is obvious because of dominance of this additional horizontal cross flow $\left(Re_f\right)$ on the Rayleigh-Taylor instability. One more observation is that the length of vertical positions of interfacial configurations shortens with rise of horizontal cross flow $\left(Re_f\right)$ for a particular time stamp. Here, the hydrodynamic force $\left(Re_f\right)$ resists the interfacial structure causing the length of vertical positions of interfacial configurations to reduce for rise in Re_f (Figure 3 (j, o, and t)).

After observation and detailed analysis for two-dimensional Rayleigh-Taylor instability problem, we have concluded more effective and prominent outcomes are found at a Re_f range of 0-5 (Figure 3) and a ρ_r range of 1.8-14.46 (Figure 4). So for this current investigation, we have chosen this range of Re_f and ρ_r in variations in microscopic interface location. But the influence of Re_f and ρ_r on vertical $\left(Y(m)\right)$ and angular $\left(\theta(degree)\right)$ positions due to the shear flow of heavier fluid is also a topic of this current investigation. Figure 4 illustrates the variation of the steady numerical contours of Rayleigh-Taylor instability for the various density ratio (ρ_r) at a particular Re_f ($Re_f = 3$). We have taken a wide range of ρ_r (1.8-14.46) for a constant Re_f $\left(Re_f = 3\right)$ to portray the variations in interfacial confriguarations. The vertical postions $\left(Y(\mathrm{m})\right)$ from intial undisturbed interface is seen to be remarkbley higher with raise of denity ratio (ρ_r) for a particular shear-layer flow $\left(Re_f = 3\right)$. Here, increase in density ratios will lead to higher momentum transfer between phases and the effect of horizontal cross flow of heavier fluid becames weakens. Therefore, development and generation of higher frequency form bubbles established which determines the growth rate of interfacial structures takes less time with rise in density ratio (ρ_r). Another important finding is that the angular postions $\left(\theta(\mathrm{degree})\right)$ which generally determined from initial undisturbed interface is gradually shifts more towards right side with rise in ρ_r for a particular Re_f $\left(Re_f = 3\right)$ (Figure 4).

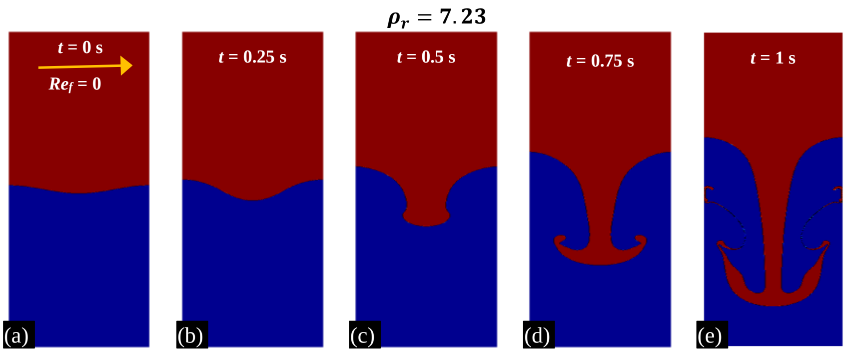

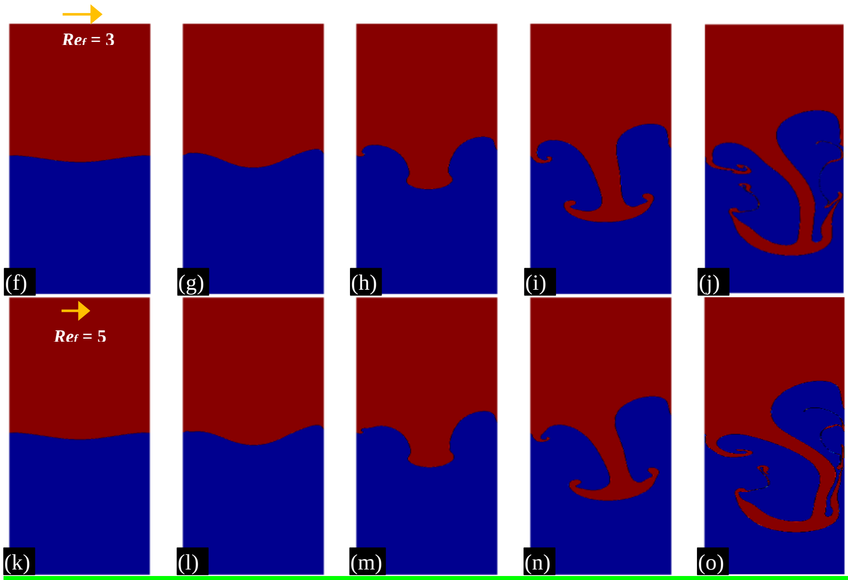

Figure 3. Variation of the temporal evolution of interfacial configuration for a particular $\rho_r = 7.23$. Row- and column-wise Re_f and t remained constant, respectively. Row 1: for $Re_f = 0$ at (a) $t = 0$ s, (b) $t = 0.25$ s, (c) $t = 0.5$ s, (d) $t = 0.75$ s, and (e) $t = 1$ s. Row 2: for $Re_f = 1.5$ at (f) $t = 0$ s, (g) $t = 0.25$ s, (h) $t = 0.5$ s, (i) $t = 0.75$ s, and (j) $t = 1$ s. Row 3: for $Re_f = 3$ at (k) $t = 0$ s, (l) $t = 0.25$ s, (m) $t = 0.5$ s, (n) $t = 0.75$ s, and (o) $t = 1$ s. Row 4: for $Re_f = 5$ at (p) $t = 0$ s, (q) $t = 0.25$ s, (r) $t = 0.5$ s, (s) $t = 0.75$ s, and (t) $t = 1$ s.

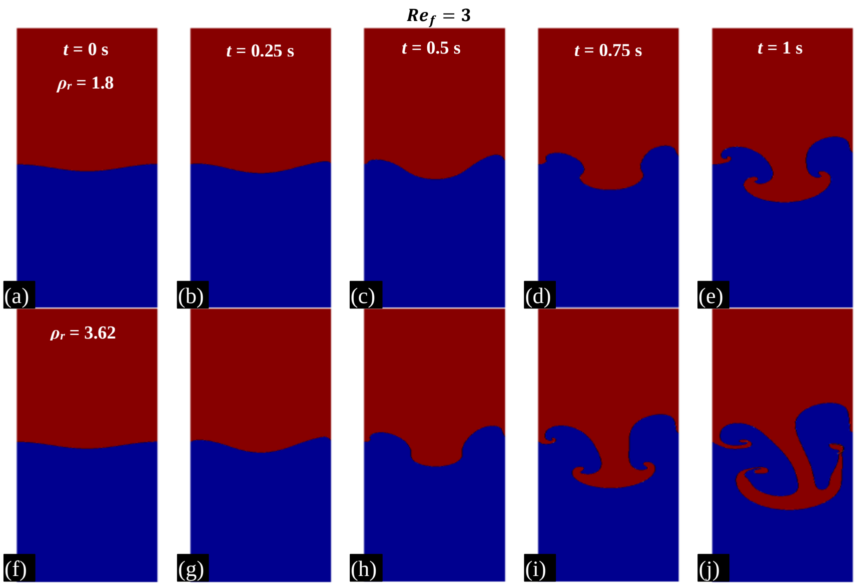

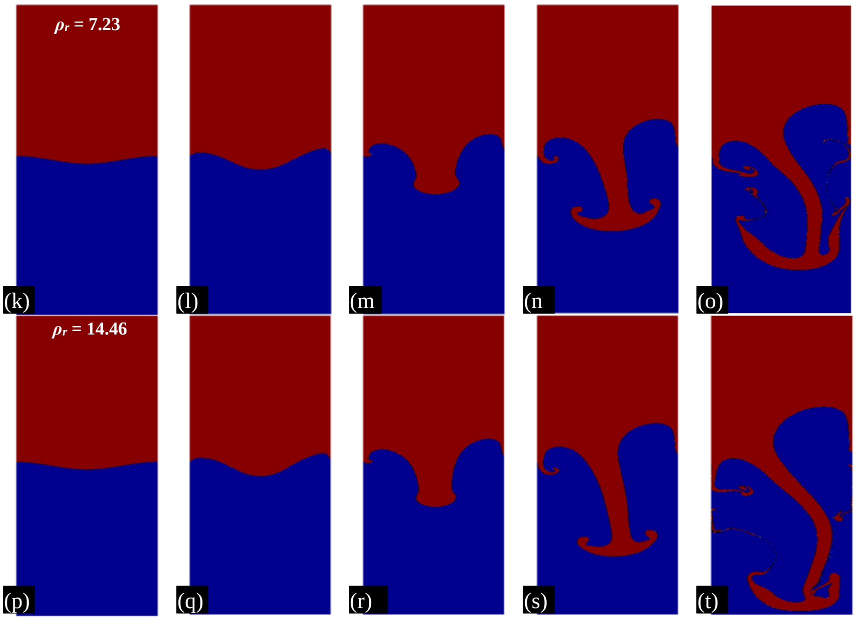

Figure 4. Variation of the temporal evolution of interfacial configuration for a particular $Re_f = 3$. Row- and column-wise ρ_r and t remained constant, respectively. Row 1: for $\rho_r = 1.8$ at (a) $t = 0$ s, (b) $t = 0.25$ s, (c) $t = 0.5$ s, (d) $t = 0.75$ s, and (e) $t = 1$ s. Row 2: for $\rho_r = 3.62$ at (f) $t = 0$ s, (g) $t = 0.25$ s, (h) $t = 0.5$ s, (i) $t = 0.75$ s, and (j) $t = 1$ s. Row 3: for $\rho_r = 7.23$ at (k) $t = 0$ s, (l) $t = 0.25$ s, (m) $t = 0.5$ s, (n) $t = 0.75$ s, and (o) $t = 1$ s. Row 4: for $\rho_r = 14.46$ at (p) $t = 0$ s, (q) $t = 0.25$ s, (r) $t = 0.5$ s, (s) $t = 0.75$ s, and (t) $t = 1$ s.

After detailed analysis about temporal evolutaion of interfacial structure of Rayleigh-Taylor instability in presence of shear-layer flow of upper medium, the vertical position $(Y(\mathrm{m}))$ of spike from initial undisturbed interface for various Re_f and ρ_r quantified against progessive time $(t(\mathrm{s}))$ is an extensive study of this present research. Presently, the penetraion rate $(Y(\mathrm{m}))$ of spike increses with progeess of time $(t(\mathrm{s}))$ for all the situations. However, the penetraion rate $(Y(\mathrm{m}))$ of spike decreases with increase of Re_f for a particualar ρ_r ($\rho_r = 7.23$) (Figure 5(a)). It is quite obvious due to strong influence of hydrodynamic force dominates over interfacial structres. As a result, the interface bents more towrads right side and also squeeze at the same time becacuse of shear-layer flow of upper medium (also observed from Figure 3). However, the percentage decrease of $Y(\mathrm{m})$ from $Re_f = 0 - 5$ is approximately 18.3% for a particular ρ_r. Figure 5(b) depicts variations in vertical positions $(Y(\mathrm{m}))$ of spike from initial undisturbed interface due to various ρ_r for a particular shear-layer flow $(Re_f = 3)$. It has been observed that depth of penetration $(Y(\mathrm{m}))$ of spike increases with increases ρ_r for a particular Re_f. The increment in depth of penetration of spike due to higher momentum transfer between phases. As a result, development and generation of higher frequency form bubbles established which determines the growth rate of spike takes less time with rise in density ratio (ρ_r). In spite of that, the percentage decrease of $Y(\mathrm{m})$ from $\rho_r = 1.8 - 14.46$ is approximately 70% for a particular Re_f.

In this present research article, we have introduced a new way of approach to representing the angular position $(\theta(\text{degree}))$ of spike from initial undisturbed interface developed due to with/without effect of horizontal cross flow (Re_f) of upper medium. The angular position $(\theta(\text{degree}))$ of spike is the angle subtended from the meeting point of the initial undisturbed interface and the vertical line passing through the centre bubble to the centre of the spike (insert Figure 6 (a)). Figures 6(a) and 6(b) demonstrates the influence of Re_f and ρ_r on angular position $(\theta(\text{degree}))$ of spike from initial undisturbed interface. The angular position $(\theta(\text{degree}))$ of spike is progressively increases with increases time and found to be more at higher Re_f and ρ_r respectively (Figure 6(a-b)). It is due to strong influence of hydrodynamic force dominates over interfacial structres. As a result, the spike bents more towrads right side for both the cases (Figures 3, 4). However, the percentage increase in angular position $(\theta(\text{degree}))$ due to a particular horizontal cross flow $(Re_f = 5)$ and density ratio $(\rho_r = 14.46)$ from $t = 0.55 - 1s$ is approximately 30% and 64% respectively.

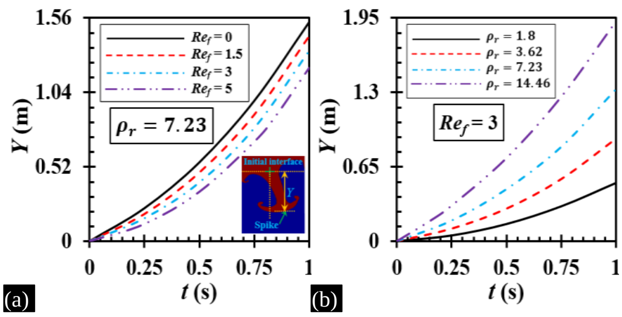

Figure 5. (a, b) Influence of Re_f and ρ_r on vertical position $(Y(\text{m}))$ of spike from initial undisturbed interface.

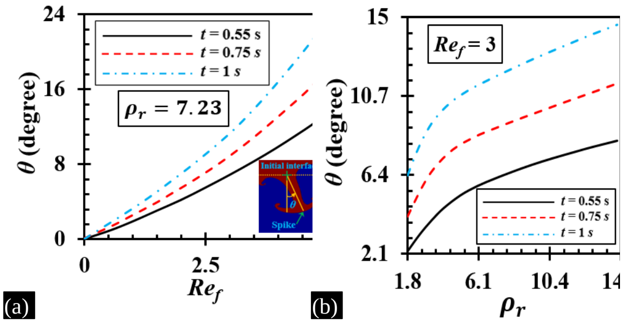

Figure 6. (a, b) Influence of Re_f and ρ_r on angular position $(\theta(\text{degree}))$ of spike from initial undisturbed interface.

Velocity vectors are thought to be a crucial tool for visualising the distribution of the flow near the interface. The velocity vectors for Rayleigh-Taylor instability in presence of shear-layer flow of upper medium are herein shown at different Re_f and ρ_r in order to elucidate the flow pattern as shown in Figure 7 (a-d). The discrepancies in the interfacial configurations due to these Re_f and ρ_r are clearly recognized in Figure 7.

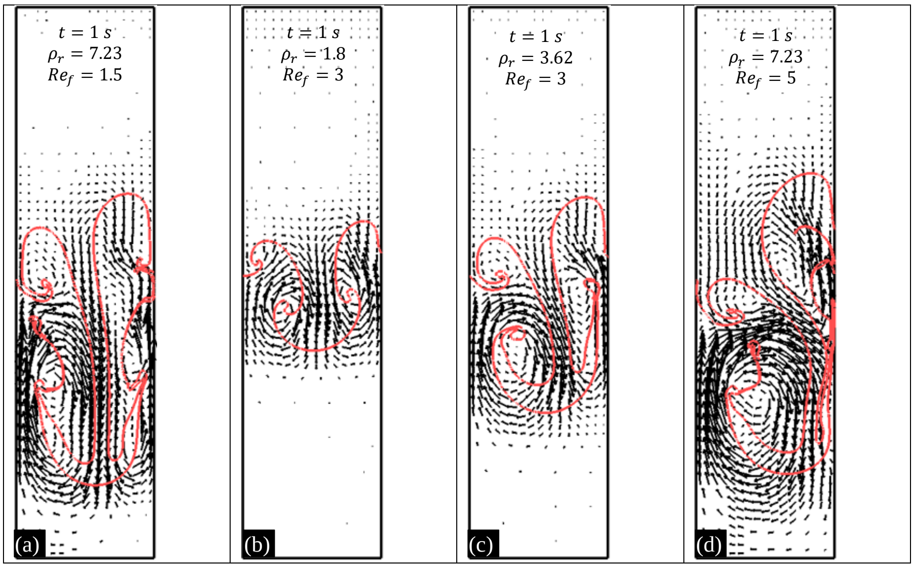

Figure 7. Flow pattern of velocity vectors at (a) $t = 1$ s, $\rho_r = 7.23$, $Re_f = 1.5$, (b) $t = 1$ s, $\rho_r = 1.8$, $Re_f = 3$, (c) $t = 1$ s, $\rho_r = 3.62$, $Re_f = 3$, and (d) $t = 1$ s, $\rho_r = 7.23$, $Re_f = 5$.

CONCLUSIONS

Comprehensive analysis of influence of horizontal cross flow (Re_f) and density ratio (ρ_r) on interfacial configuration to predict the profile and structure of interface of Rayleigh-Taylor instability problem has been investigated. In this paper, we have discussed the effect of Re_f and ρ_r on vertical $(Y(\text{m}))$and angular $(\theta(\text{degree}))$ positions of spike from initial undisturbed interface. Apart from this, fluid properties and the concept of two phase flow are the subjects of this present investigation. Lastly, we have illustrated the mechanisms of all interfacial activity and flow distributions by displaying the velocity vectors at various Re_f and ρ_r.

Acknowledgements

The authors would like to thank and acknowledge the Science and Engineering Research Board (SERB), Department of Science and Technology (DST), Government of India, for providing financial support to carry out research work via the Start-up Research Grant (SRG) scheme (No. SRG/2019/001438).

REFERENCES

1. Sharp DH. Overview of Rayleigh-taylor instability. Los Alamos National Laboratory (LANL), Los Alamos, NM (United States); 1983 Jan 1.
2. Rayleigh. Investigation of the character of the equilibrium of an incompressible heavy fluid of variable density. Proceedings of the London mathematical society. 1882 Nov 1;1(1):170-7.
3. Taylor GI. The instability of liquid surfaces when accelerated in a direction perpendicular to their planes. I. Proceedings of the Royal Society of London. Series A. Mathematical and Physical Sciences. 1950 Mar 22;201(1065):192-6.
4. Keskinen MJ, Szuszczewicz EP, Ossakow SL, Holmes JC. Nonlinear theory and experimental observations of the local collisional Rayleigh-Taylor instability in a descending equatorial spread F ionosphere. Journal of Geophysical Research: Space Physics. 1981 Jul 1;86(A7):5785–92.

5. Veynante D, Vervisch L. Turbulent combustion modeling. Progress in energy and combustion science. 2002 Mar 1;28(3):193–266.
6. Debnath L. Nonlinear Water Waves, Academic P ress. Inc., Boston, M A. 1994.
7. Brecht SH, Papadopoulos K. Cross field jetting of energetic ions produced by Rayleigh-Taylor instability. Interim report. Naval Research Lab., Washington, DC (USA); 1979 Oct 3.
8. Ribeyre X, Tikhonchuk VT, Bouquet S. Compressible Rayleigh–Taylor instabilities in supernova remnants. Physics of Fluids. 2004 Dec 1;16(12):4661–70.
9. Buchler JR, Livio M, Colgate SA. Supernova explosions-the role of a Rayleigh-Taylor instability. InInternational Astronomical Union Colloquium 1980 Aug (Vol. 58, pp. 571–577). Cambridge University Press.
10. Hester JJ. The Crab Nebula: an astrophysical chimera. Annu. Rev. Astron. Astrophys.. 2008 Sep 22;46(1):127–55.
11. Tian JW, Yuan XJ. Numerical simulation of Rayleigh-Taylor instability with large density ratios based on RKDG method. Applied Mechanics and Materials. 2013 Dec 12; 423:1751–6.
12. Rahmat A, Tofighi N, Shadloo MS, Yildiz M. Numerical simulation of wall bounded and electrically excited Rayleigh–Taylor instability using incompressible smoothed particle hydrodynamics. Colloids and Surfaces A: Physicochemical and Engineering Aspects. 2014 Oct 20; 460:60–70.
13. Ding H, Spelt PD, Shu C. Diffuse interface model for incompressible two-phase flows with large density ratios. Journal of Computational Physics. 2007 Oct 1;226(2):2078–95.
14. Zu YQ, He S. Phase–field-based lattice Boltzmann model for incompressible binary fluid systems with density and viscosity contrasts. Physical Review E—Statistical, Nonlinear, and Soft Matter Physics. 2013 Apr;87(4):043301.
15. Xiang G, Ren Z, Kim S, Wang B. Numerical analysis on the disintegration of gas-liquid interface in two-phase shear-layer flows. Aerospace Science and Technology. 2020 Mar 1;98:105710.
16. Panda SK, Rana BK, Kumar P. Competition of roller rotation and horizontal crossflow to control the free surface cusp-induced air entrainment. Physics of Fluids. 2021 Nov 1;33(11).
17. Panda SK, Rana BK, Kumar P. Film flow and air entrainment around partially submerged rotating roller with a steady flow of air: A numerical approach. InProceedings of the 26thNational and 4th International ISHMT-ASTFE Heat and Mass Transfer Conference December 17-20, 2021, IIT Madras, Chennai-600036, Tamil Nadu, India 2021. Begel House Inc.
18. Panda SK, Rana BK, Kumar P. Film flow and air entrainment around partially submerged rotating roller with a steady flow of air: A numerical approach. InProceedings of the 26thNational and 4th International ISHMT-ASTFE Heat and Mass Transfer Conference December 17–20, 2021, IIT Madras, Chennai-600036, Tamil Nadu, India 2021. Begel House Inc.
19. Panda SK, Rana BK. Influence of the immersion ratio of a revolving roller on the film coating and entrainment dynamics. Industrial & Engineering Chemistry Research. 2023 Apr 10;62(15):6285–300.
20. Panda SK, Rana BK. Behavior of gas entrainment inside viscous pool due to combined influence of symmetric rotational field and freestream flow of air. Journal of Fluids Engineering. 2023 Feb 1;145(2):021402.
21. Panda SK, Rana BK. Gaseous entrainment dynamics in a viscous pool due to combined influence of asymmetric rotational field and crossflow of air. Journal of Fluids Engineering. 2023 Feb 1;145(2):021401.
22. Panda SK, Rana BK. Interfacial dynamics around a swirling roller in the presence of oppositely imposed horizontal crossflows. Journal of Fluids Engineering. 2024 Jan 1;146(1).
23. Panda SK, Rana BK. Formation and Development of Cusp-Induced Air Entrainment Caused by Fully Submerged Rotary Solid Roller: A Numerical Investigation. In Recent Advances in Thermo fluids and Manufacturing Engineering: Select Proceedings of ICTMS 2022 2022 Oct 1 (pp. 103–112). Singapore: Springer Nature Singapore.

24. Panda SK, Rana BK. Numerical Analysis of Gas Entrainment in the Viscous Liquid Pool Developed by a Counter-Rotating Pair of Fully Submerged Rollers. In Recent Advances in Thermofluids and Manufacturing Engineering: Select Proceedings of ICTMS 2022 2022 Oct 1 (pp. 3-11). Singapore: Springer Nature Singapore.
25. Panda SK, Rana BK, Kumar P. Entrainment in multifluid systems, and rotation induced occurrences. European Journal of Mechanics-B/Fluids. 2022 Nov 1; 96:156–72.
26. Panda SK, Rana BK. Numerical simulation, and analytical prediction on the development of entrained air filament caused by the combined effect of rotational field and free stream flow. Industrial & Engineering Chemistry Research. 2022 Jun 22;61(26):9456–73.
27. Panda SK, Rana BK. Rotational flux influenced cusp entrainment in a viscous pool. Physics of Fluids. 2022 Oct 1;34(10).
28. Panda SK, Rana BK. Characterization of air entrainment using a pair of vertically aligned revolving rollers. Industrial & Engineering Chemistry Research. 2023 Jan 9;62(2):998–10
29. Popinet S. Gerris: a tree-based adaptive solver for the incompressible Euler equations in complex geometries. Journal of computational physics. 2003 Sep 20;190(2):572–600.
30. Popinet S. An accurate adaptive solver for surface-tension-driven interfacial flows. Journal of Computational Physics. 2009 Sep 1;228(16):5838–66.